TAI, HENRY, M.S. Calcium and Chloride Function in Oxygen Evolution by Photosystem II through Bisubstrate Enzyme Kinetics and EPR Spectroscopy of Fluoride Inhibition. (2013)
Directed by Dr. Alice Haddy. 50 pp.

Photosystem II (PSII) is the light-harvesting water oxidase of thylakoid membranes. The catalytic center where oxygen forms in PSII is located at the manganese cluster, Mn_4O_5Ca, which is highly conserved throughout nature as seen in cyanobacteria and in higher plants. PSII requires both Ca^{2+} and Cl^- for oxygen evolution activity, but their roles in catalysis and the interactions between the two cofactors are not well understood. Two studies were done to elucidate the interaction between Ca^{2+} and Cl^-.

The first study investigated the interdependence of Ca^{2+} and Cl^- activation of oxygen evolution in spinach PSII using enzyme kinetics analyses at the low pH of 5.5. At this pH substrate inhibition at high chloride concentrations was observed, with a decrease in inhibition when the Ca^{2+} concentration increased. The K_I for Cl^- doubled from 31 mM at 0.2 mM Ca^{2+} to 68 mM at 5 mM Ca^{2+}. Bisubstrate enzyme kinetics analyses of activation showed that the Michaelis constants were 0.26 mM for $Ca^{2+}$and 0.97 mM for Cl^- and the dissociation constants were 0.31 mM for Ca^{2+} and 1.15 mM for Cl^-.

The second study investigated the effect of fluoride, a competitive inhibitor of Cl^- activation, on the tyrosine Z (Tyr_Z) radical that is involved in electron transfer from the manganese cluster. Using electron paramagnetic resonance (EPR) spectroscopy, the Tyr_Z radical was observed at 77 K in fluoride-inhibited PSII, indicating that electron transfer

was blocked. The study showed a positive correlation in Tyr_Z radical formation with increasing F^- concentration which is believed to indicate formation of the $S_2Y_Z\bullet$ state.

CALCIUM AND CHLORIDE FUNCTION IN OXYGEN EVOLUTION BY PHOTOSYSTEM II THROUGH BISUBSTRATE ENZYME KINETICS AND EPR SPECTROSCOPY OF FLUORIDE INHIBITION

by

Henry Tai

A Thesis Submitted to
the Faculty of the Graduate School at
The University of North Carolina at Greensboro
in Partial Fulfillment
of the Requirements for the Degree
Master of Science

Greensboro
2013

Approved by

_____
Committee Chair

APPROVAL PAGE

This thesis has been approved by the following committee of the Faculty of the Graduate School at the University of North Carolina at Greensboro.

Committee Chair _____

Committee Members _____

_____

_____
Date of Acceptance by Committee

_____
Date of Final Oral Examination

ACKNOWLEDGMENTS

This research was funded by a grant from the National Science Foundation (MCB-0950285). I wish to thank Dr. Alice Haddy for all the help and guidance throughout the MS Chemistry program. I also want to thank Jeremiah Johnston for providing preliminary experiments on calcium and chloride dependence of oxygen evolution.

TABLE OF CONTENTS

Page

LIST OF TABLES

Page

LIST OF FIGURES

Page

LIST OF ABBREVIATIONS

chl	chlorophyll
EPR	electron paramagnetic resonance
MES	2-(N-morpholino)ethanesulfonic acid.
PPBQ	phenyl-*p*-benzoquinone
PSI	photosystem I
PSII	photosystem II
Tyr	tyrosine

CHAPTER I

INTRODUCTION

Photosynthesis is one of the most essential biochemical reactions that support life on earth. Light energy is converted into chemical energy for biological processes. Photosynthesis occurs in two sets of reactions called the light and the dark reactions, which take place in the chloroplast of higher plants and also in cyanobacteria. The light reactions occur in the thylakoid membrane and involve two major protein structures know as photosystem II (PSII) and photosystem I (PSI). The dark reactions occur in the stroma of the chloroplast where CO_2 is converted into sugars. The overall reactions of photosynthesis are summarized in the equation below.

$$6CO_2 + 6H_2O \xrightarrow{h\nu} 6O_2 + C_6H_{12}O_6$$

PSII absorbs light and uses the energy to convert H_2O to O_2 (Vinyard et al, 2013). The actual water splitting site of PSII contains a manganese cluster which consists of a cluster of four manganese ions, five oxygen atoms, and one calcium cofactor (Umena et al., 2011). In addition to the calcium cofactor, chloride is needed for the reaction to proceed forward (Yocum, 2007). Two chlorides are located in close proximity to the manganese cluster (Kawakami et al, 2009). The actual mechanism is still unclear as to exactly how Ca^{2+} and Cl^- are involved in catalysis. An amino acid residue, tyrosine Z,

also plays an important role in the oxidation of water by assisting electron transfer from the manganese cluster to the light absorption site, P680 (Barry and Babcock, 1984).

This study looks further into the mechanism of conversion of H_2O into O_2 at the manganese cluster to help elucidate the mechanism of the oxygen evolving reaction. The first part examines oxygen evolution by PSII at the low pH of 5.5 using bisubstrate enzyme kinetics to simultaneously characterize Ca^{2+} and Cl^- activation and test for their possible interaction. In addition Cl^- inhibition effects are modeled using substrate inhibition enzyme kinetics. In the second part of the study, fluoride treatment of PSII is used to look at the blockage of electron transfer from the Mn cluster. This is shown by formation of the tyrosine Z radical which is observed using electron paramagnetic resonance (EPR) spectroscopy. EPR spectroscopy is able to capture signals from the tyrosine radical and manganese oxidation states because they have unpaired electrons. The effects of fluoride, which competes with chloride activation, are similar to those of Ca^{2+} depletion.

Background

Light Reaction Z-Scheme – Photosynthesis light reactions are promoted by light absorption by two proteins complexes, photosystem II and photosystem I. The reactions of these proteins can be summarized in a diagram called the Z-scheme, shown in Figure 1. This diagram displays the energy levels of the various electron transfer centers, with H_2O as electron donor and NADPH as the final reduced product. The two photosystem enzymes absorb light with a maximum absorption at 680 nm for PSII and 700 nm for PSI. Electrons from the splitting of water molecules are transferred to Tyr_Z and then to

P680. The P680 site promotes the electron transfer using light energy with a series of subsequent steps to Q_A and then to Q_B as the final electron acceptor in PSII. The electron is then transferred via the cytochrome b_6f complex to PSI where the absorption of light energy at P700 is also used to help electron transfer. These reactions in PSI eventually reduce NADP, which is the final electron acceptor. This electron transfer process is coordinated with proton transfer to produce a pH gradient across the thylakoid membrane that drives the production of ATP, the major source of chemical energy for the cell (Hillier and Babcock, 2001; Schönknecht et al., 1995).

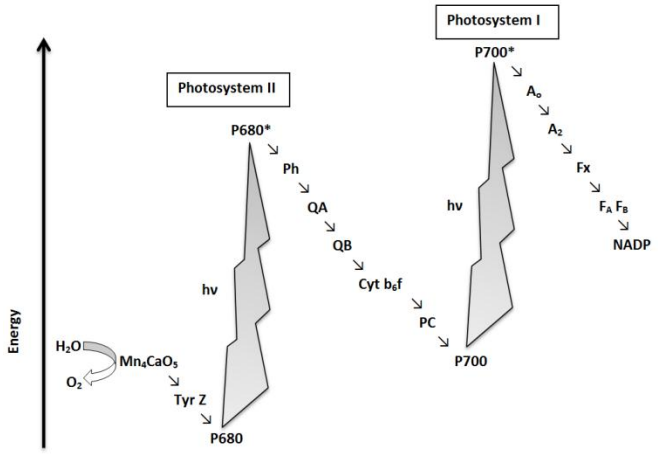

Figure 1. The Z-Scheme. This shows the energy levels of the electron transfer process in photosynthesis starting from water in PSII to NADP in PSI (redrawn from Hillier and Babcock, 2001).

Photosystem II - Oxygen evolution refers to the biochemical redox reaction in PSII of plants and cyanobacteria where H_2O is converted to O_2 using light energy. The half reaction is shown.

$$2H_2O \xrightarrow{h\nu} O_2 + 4H^+ + 4e^-$$

This reaction is responsible for most if not all of the oxygen in the Earth's atmosphere. Photosystem II (PSII) is a thylakoid membrane-embedded protein complex of about 350 kDa molecular weight consisting of about 20 major subunits (Umena et al. 2011). The crystal structure of the PSII dimer from the thermophilic cyanobacterium, *Thermosynechococcus elongatus*, is shown in Figure 2.

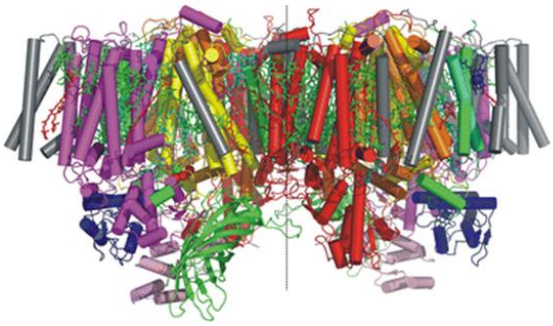

Figure 2. PSII Crystal Structure. The homodimeric structure of photosystem II includes various protein subunits and cofactors required for oxygen evolution (Kern and Renger, 2007)

In higher plants such as spinach, there are three extrinsic subunits located on the thylakoid lumenal side of PSII known as PsbO (33 kDa), PsbP (23 kDa), and PsbQ (17 kDa). The subunits are not ligated to the Mn_4Ca complex; they provide an accessibility barrier to the manganese cluster for inorganic ions (Seidler, 1996). The PsbO subunit is associated with stabilization of manganese at the active site. The function of PsbP and PsbQ helps the manganese cluster retain Ca^{2+} and Cl^- for higher oxygen evolution activity (Kakiuchi, 2012). The PsbP and PsbQ subunits are easily removed by high NaCl concentration which causes the calcium and chloride cofactors to also be removed easily

from the structure. With the extrinsic subunits removed, the binding of the cofactors can be controlled using various buffer environments (Ifuku et al., 2011).

Kok Cycle – The Kok S-state cycle in Figure 3 depicts the manganese cluster redox cycle during catalytic water splitting (Kok et al. 1970). The manganese cluster cycles through five different S-states represented as S_n, where n = 0, 1, 2, 3, or 4. The progression of S-states from S_0 to S_4 requires absorption of one photon at P680 for one oxidation step of the manganese in the cluster. During the step from S_4 to S_0, the manganese cluster is reduced back to the S_0 state due to the formation and the release of O_2 from the site. Hydrogen ions are thought to be released during S_0, S_2, S_3, and S_4 (Dau and Haumann, 2007). S_1 is the long term dark stable state and there is no release of a proton upon going from S_1 to S_2. One full Kok cycle results in the consumption of two H_2O molecules for the evolution of one O_2 molecule and the release of four protons (Dau and Haumann, 2007).

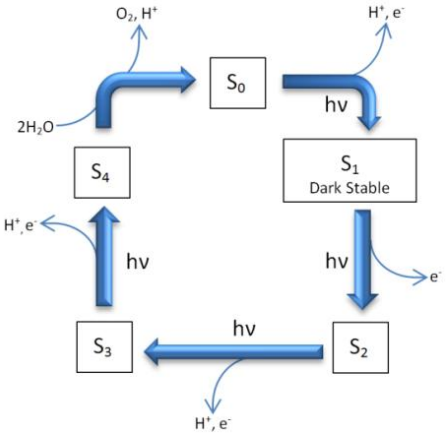

Figure 3. Kok Cycle. The cycle shows different manganese S-states during the conversion of H_2O to O_2 in PSII (redrawn from Kok et al., 1970).

Calcium and Chloride – The Ca^{2+} and Cl^- ions required for oxygen evolution have been located within the catalytic complex by X-ray diffraction studies (Figure 4). As a part of the manganese cluster, calcium has a distance of 3.3 Å and 3.8 Å away from the two nearest manganese (Umena et al., 2011). Although a part of the cluster it is relatively labile. There are two chloride ions located in close proximity to the manganese cluster. One of the chlorides is located 6.7 Å away and the other is 7.4 Å away from the nearest manganese (Umena et al, 2011). Chloride may have a role in maintaining the structure of the manganese cluster (Kawakami et al., 2009). It is thought that chloride helps with the release of protons (Boussac et al., 2012).

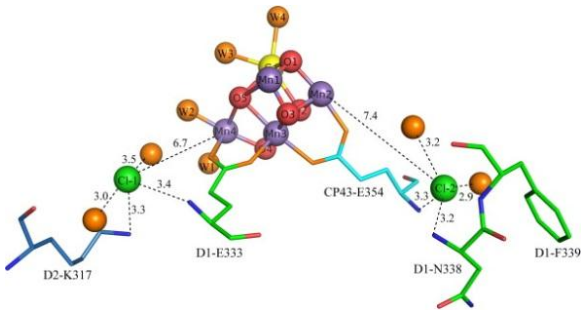

Figure 4. Manganese Cluster. The oxygen evolving complex of PSII, where water is oxidized into molecular oxygen, consists of four manganese ions (purple) and a calcium ion (yellow). The two chloride (green) binding sites were found close to the manganese cluster. The distances are given in Å (Kawakami et al., 2011).

Tyrosine Radicals – A Tyr residue, D1-Tyr-161, called Tyr_Z plays an important part in the transfer of electrons from the manganese cluster to the light absorbing complex, P680 (Haumann et al., 1999). In fact two tyrosine residues, D2-Tyr-160 called Tyr_D and Tyr_Z, can donate electrons to P680, thereby forming radicals (Barry and Babcock, 1987). Although two Tyr radicals can be observed, only Tyr_Z participates in

linear electron transfer from the H_2O to Q_A/ Q_B (Ayala et al., 1999). At the same time as an electron is transferred from Tyr_Z to P680, Tyr_Z transfers a proton to D1-His-190 to remain neutral (Saito, 2011). When Tyr_Z is reduced by the Mn cluster, the proton transfers back from D1-His190 to the tyrosine ring. Tyr_D undergoes a similar deprotonation when it is reduced, transferring a proton to acceptor D2-His 189. When it donates an electron to P680, however, there is no immediate electron donor to Tyr_D, so it can remain a radical for much longer periods of time (Saito, 2013).

Enzyme Kinetics

Michaelis-Menten Kinetics - The Michaelis-Menten equation describes the rate of product formation from substrate by an enzyme, as shown in the chemical equation below.

$$E + S \underset{k_{-1}}{\overset{k_1}{\rightleftharpoons}} ES \overset{k_{cat}}{\rightarrow} E + P$$

Here E is the enzyme, S is the substrate, ES is the enzyme-substrate complex, and P is the product. The rate equation is

$$v = \frac{V_{Max}[S]}{K_M + [S]}$$

where v is the reaction rate, V_{max} is the maximum rate ($V_{max} = k_{cat}E_{tot}$ and E_{tot} is the total concentration of enzyme), K_m is the Michaelis constant ($K_m = \frac{k_{cat}+k_{-1}}{k_1}$), and $[S]$ is the substrate concentration. This is the simplest possible description of the rate of an

enzymatic reaction, but many enzymes follow this kinetics model. Although water is the true substrate of oxygen evolution by PSII, the amount of water present in the solvent or environment is too great to control for kinetics experiments. As it turns out, the activators, Ca^{2+} and Cl^- can be treated as substrates for use in a Michaelis-Menten kinetics analysis (Bryson et al, 2005).

The Lineweaver-Burk plot is another way to depict substrate dependence of catalytic rates in enzyme kinetics. The equation is the inverse of the Michaelis-Menten rate equation, as shown below

$$\frac{1}{v} = \frac{K_M}{V_{Max}[S]} + \frac{1}{V_{max}}$$

The graph of 1/v versus 1/[S] is a linear plot in which the y intercept = $1/V_{max}$ and the x intercept = $-1/K_m$.

Substrate Inhibition by Cl^- - For the chloride dependence of oxygen evolution at pH 5.5, the data were found to show inhibition of oxygen evolution at high Cl^- concentration as will be shown in Results and Discussion. This required that the Michaelis-Menten equation include a substrate inhibition term. In addition a constant V_0 that represents the activity at zero Cl^- concentration was included in the equation as follows.

$$(PSII) + (Cl^-) \underset{k_{-1}}{\overset{k_{+1}}{\rightleftharpoons}} (PSII)(Cl^-) \overset{k_{+2}}{\rightarrow} (PSII) + Product$$

$$\uparrow\downarrow K_I$$

$$(PSII)(Cl^-)_2$$

$$v = \frac{V_{Max}\,[Cl^-]}{[Cl^-] + K_M + \frac{[Cl^-]^2}{K_I}} + V_0$$

Ordered and Random Sequential Bisubstrate Kinetic Models - Enzymes that require two substrates to produce a product can be analyzed using a bisubstrate model. Ordered and random sequential bisubstrate kinetic models can be used for this analysis to obtained global constants for both of the substrates. In the ordered sequential model one substrate must bind before the second substrate in a specific order. The equations below show the ordered sequential model and the corresponding rate equation (Marangoni, 2003).

$$(PSII) \overset{A}{\rightleftharpoons} (PSII)A \overset{B}{\rightleftharpoons} (PSII)AB \rightarrow (PSII) + Product$$

$$\frac{1}{v} = \frac{1}{V_{Max}}\left(1 + \frac{K_M(B)}{[B]}\right) + \frac{1}{[A]V_{Max}}\left(K_M(A) + \frac{K_S(A)K_M(B)}{[B]}\right)$$

where A = Cl^-, B = Ca^{2+}

In the random sequential model either substrate can bind to the enzyme first resulting in two possible paths. Both pathways are taken into account as shown in the reaction and rate equation as shown (Marangoni, 2003).

$$(PSII) \underset{B}{\overset{A}{\rightleftharpoons}} (PSII)A \underset{A}{\overset{B}{\rightleftharpoons}} (PSII)AB \rightarrow (PSII) + Product$$

$$\frac{1}{v} = \frac{1}{V_{Max}}\left(1 + \frac{K_M(B)}{[B]}\right) + \frac{1}{[A]V_{Max}}\left(\frac{K_S(A)K_M(B)}{K_S(B)} + \frac{K_S(A)K_M(B)}{[B]}\right)$$

where A = Cl^-, B = Ca^{2+}, and $K_S(A)K_M(B) = K_S(B)K_M(A)$

Both of these equations can be solved for the individual constant using the slopes and the y-intercepts from the Lineweaver-Burk plot. The slopes and y-intercepts from the Lineweaver-Burk plot are both plotted against 1/[Ca^{2+}] or 1/[B]. The "slope versus 1/[Ca^{2+}] plot" corresponds to the equation

$$Slope = \frac{1}{V_{Max}}\left(K_M(A) + \frac{K_S(A)K_M(B)}{[B]}\right) \text{ or } Slope = \frac{1}{V_{Max}}\left(\frac{K_S(A)K_M(B)}{K_S(B)} + \frac{K_S(A)K_M(B)}{[B]}\right)$$

Therefore its slope, called the secondary slope, is $\frac{K_S(A)K_M(B)}{V_{Max}}$ and its intercept, the secondary intercept, is $\frac{K_M(A)}{V_{Max}}$ for the ordered sequential model or $\frac{K_S(A)K_M(B)}{V_{Max}K_S(B)}$ for the random sequential model. Similarly the "y-intercept versus 1/[Ca^{2+}] plot" corresponds to the equation

$$y - intercept = \frac{1}{V_{Max}}\left(1 + \frac{K_M(B)}{[B]}\right)$$

Therefore the secondary slope of the plot of y-intercept versus 1/[Ca^{2+}] is $\frac{K_M(B)}{V_{Max}}$ and its secondary intercept is $\frac{1}{V_{Max}}$. The global V_{Max} and individual Michaelis constants and dissociation constants for both Cl^- and Ca^{2+} are thereby solved.

Electron Paramagnetic Resonance (EPR) Spectroscopy

Basics of EPR - EPR spectroscopy is a technique used to study molecular systems with one or more unpaired electrons. EPR spectroscopy looks at the electron spin transitions induced by microwave radiation. Because an unpaired electron is required, EPR is only able to be used to study a limited number of species such as organic and inorganic free radicals and many transition metals. This limitation to paramagnetic species makes EPR very specific, thus most solvents and matrices do not interfere with EPR spectra. In proteins, there are various metals and amino acids that help catalyze reactions in biological processes. In PSII studies, EPR is often used to observe Tyr_D, Tyr_Z, and various oxidation states of the Mn cluster.

The basis of EPR spectroscopy is that an electron can take on two spin states, which correspond to orientations of the spin magnetic moment with quantum numbers, m_s = +½ and m_s = -½. Application of a magnetic field is able to differentiate between the two electron spins giving rise to discrete energy states. The energies of the spin states of the electron are given in the equation below:

$$E = g\mu_B B_0 m_s = \pm ½ g\mu_B B_0$$

where g is the g-factor, μ_B is the Bohr magneton, and B_0 is the external magnetic field strength. A transition between the two states is induced by microwave radiation and corresponds to the energy given in the equation below.

$$\Delta E = g\mu_B B_0$$

Detecting the Tyrosine Radicals – The Tyr_Z radical plays an important role in the transfer of electrons from the manganese cluster to P680. During illumination of PSII, electrons from P680 are transferred to pheophytin, which then passes the electrons down the electron transfer chain as mentioned in the Z-scheme. $P680^+$ then picks up another electron from the Tyr_Z residue, thus forming the Tyr_Z radical. Both Tyr_D and Tyr_Z radicals are induced by illumination, but the Tyr_Z radical decays within milliseconds because electron transfer from the Mn cluster is very quick (Ayala et al., 1999), while the Tyr_D radical is stable for hours due to the farther distance from the manganese cluster (Barry, 1995). Therefore the Tyr_Z radical is generally not observable in active samples using EPR spectroscopy, whereas the more stable Tyr_D, can be seen by EPR spectroscopy.

EPR Spectroscopy of Fluoride Treated PSII – Fluoride has been shown to inhibit oxygen evolution activity in PSII, by competing with activating Cl^- (Kuntzleman and Haddy, 2009). In addition some characteristics of fluoride treatment are similar to Ca^{2+} depletion of PSII (Baumgarten et al., 1990; DeRose et al., 1995; Kuntzleman and Haddy, 2009). The Cl^- competition can be seen in F^- treated PSII as enhancement of the EPR signal at g = 4.1 and suppression of the multiline signal at g = 2.0, both of which are from

the manganese cluster in the S_2 state (DeRose et al., 1995). Also fluoride treated PSII shows a broad g = 2 signal, called the $S_2Y_Z^{\bullet}$ signal, upon illumination at liquid He temperatures due to the interaction of the Tyr_Z radical with the S_2 state manganese cluster (DeRose et al., 1995). This signal is similar to the $S_2Y_Z^{\bullet}$ signal that is observed in Ca^{2+} depleted PSII and suggests that electron transfer from the manganese cluster to Tyr_Z is blocked. It is thought that when fluoride is present, electrons are not able to transfer to the Tyr_Z residue, resulting in inhibition of water oxidation. The effect of fluoride causes a buildup of the Tyr_Z radical, which is normally not observed in active samples.

CHAPTER II

OVERVIEW OF EXPERIMENTS

Enzyme Kinetics of Cl^- and Ca^{2+} Effects at pH 5.5

In order to determine the effects of Cl^- and Ca^{2+} dependence, enzyme kinetics experiments were undertaken using oxygen evolution assays. Inhibition by Cl^- at high concentrations is seen at pH 5.5, but is not observable at pH 6.3. Experiments were conducted by varying the concentrations of the cofactors Cl^- and Ca^{2+} during oxygen evolution assays. The data were analyzed via Michaelis-Menten and Lineweaver Burk plots to determine both activation and inhibition effects of Cl^- at various Ca^{2+} concentrations. Using secondary plots extracted from the V_{max} and K_m values, both the random and ordered sequential binding models were used to obtain global constants for activation by Cl^- and Ca^{2+}.

Fluoride Inhibition of Cl^- Activation of Oxygen Evolution

An adjacent study was performed using fluoride treated PSII samples to observe the light-induced Tyr_Z EPR signal. The signal is observable because F^- apparently prevents electron transfer from the Mn cluster to Tyr_Z. A method was worked out to subtract the Tyr_D signal to quantify the Tyr_Z signal following light exposure experiments. Following those preliminary experiments, intact PSII samples and NaCl-washed PSII samples treated with various concentrations of F^- were used to observe the Tyr_Z radical signal.

CHAPTER III

MATERIALS AND METHODS

Reagents

The reagents used throughout the study were from Fisher Scientific, Fairlawn NJ, or Sigma Aldrich. The water used for solutions and buffers was from the Barnstead NANOpure Diamond Water Purification System.

Intact PSII

Photosystem II enriched thylakoid membrane fragments were prepared from fresh spinach (obtained from the local grocery store, Harris Teeter). The extraction of the PSII was achieved using Triton X-100 detergent, resulting in the removal of other membrane protein complexes and leaving the membrane fragments containing intact PSII centers (Berthold et al., 1981). These intact PSII centers were capable of evolving oxygen in the presence of an electron acceptor, such as phenyl-*p*-benzoquinone (PPBQ). The detergent was washed out by centrifugation with the Beckman Avanti J-25 centrifuge with multiple dilutions of buffer containing 20 mM MES-NaOH (2-(N-morpholino)ethanesulfonic acid), pH 6.3, 0.4 M sucrose, and 15 mM NaCl. The buffer was prepared at pH 6.3, which has been experimentally shown to produce the maximum activity of PSII. The PSII sample was frozen in liquid nitrogen for storage.

NaCl-washed PSII Lacking PsbP and PsbQ

PSII lacking the extrinsic subunits PsbP and PsbQ were prepared from intact PSII. The photosystem II samples prepared using this method is referred to as NaCl-washed PSII. In this preparation, intact PSII was suspended in buffer containing 20 mM MES-NaOH, pH 6.3, and 0.4 M sucrose, with an addition of 1.5 M NaCl to remove the two extrinsic subunits (Cammarata and Cheniae, 1987; Miyao and Murata 1985). The high NaCl concentration was removed with multiple washes by centrifugation in buffer containing 20 mM MES-NaOH, pH 6.3, and 0.4 M sucrose. The wash buffer and the final buffer did not contain Cl^- or Ca^{2+}. The sample was also stored in liquid nitrogen.

Measuring Chlorophyll Concentration

In PSII studies, measurements of the concentration of the protein are not practical because of the high chlorophyll and lipid content. The standard method of quantification is measurement of the chlorophyll concentration. There is a ratio of about 250 chlorophylls per PSII in the standard intact PSII preparation which includes antenna proteins (Smith et al., 1990). Although PSI also has chlorophyll, the Triton X-100 purification method removes almost all PSI from the prep. To measure chlorophyll, it was first extracted from the PSII sample using 80% acetone. UV/Vis spectroscopy was used to measure the green chlorophyll at 645 nm and 663 nm, the maxima for chlorophyll b and chlorophyll a, respectively (Arnon, 1949). Molar absorptivities were then used to calculate total chlorophyll.

Oxygen Evolution Assay

The buffers used for the PSII sample included 0.4 M sucrose and 20 or 50 mM MES. Oxygen evolution assays were used to study the activity of PSII during illumination. Figure 5 shows the experimental setup for oxygen evolution assays. The assays were carried out in a standard buffer under dim light at 25°C with the addition of Ca^{2+} and/or Cl^- as indicated. The light source initiating photosynthesis provided saturating light intensity (Dolan-Jenner Fiberlite 180 illuminator and School Master Graflex SVE Projector). The sample concentration for the experiment was about 20 μg chlorophyll in 1 mL solution. Nitrogen gas was used to purge the excess oxygen gas from the sample. A Yellow Springs Instruments Clark-type O_2 electrode model 5330 was used to measure the O_2 concentration as it was evolved. The electrode was connected to the Vernier Instruments LabPro interface, which was connected to a computer with the Logger Pro program for analysis. About 1 mM of PPBQ was used as the electron acceptor of PSII in order for multiple turnovers of the reaction to take place. For intact PSII samples, Ca^{2+} was omitted from the buffer, whereas it was required for NaCl-washed PSII to show the maximum activity due to the loss of PsbP and PsbQ subunits. The typical maximum rate for intact PSII was 700-800 μmol O_2/mg Chl/hr and for PSII lacking PsbP and PsbQ was 300-400 μmol O_2/mg Chl/hr.

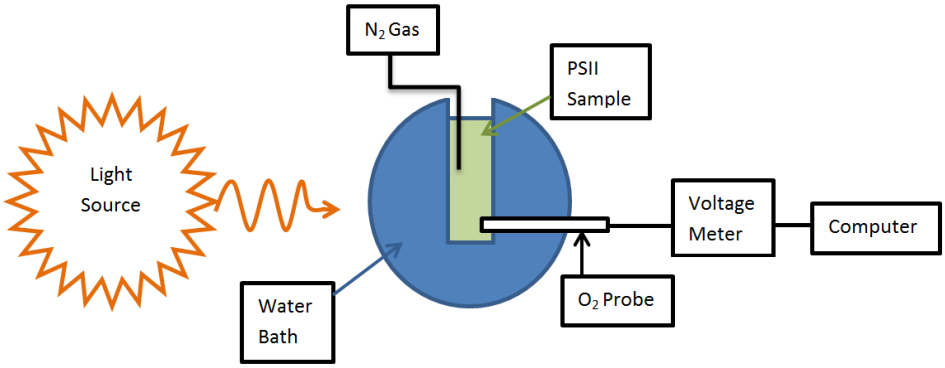

Figure 5. Oxygen Evolution Apparatus. The apparatus used for oxygen evolution assays of PSII with activation by light. Nitrogen gas was used to purge oxygen from the sample. An O_2 probe was used to detect the evolving O_2 as a voltage. The computer then converted the signal to O_2 concentration.

Preparing Samples for EPR spectroscopy

Both intact PSII and NaCl-washed PSII were used to prepare EPR samples for the study. The PSII samples were first washed three times by centrifugation and resuspended using buffer containing 20 mM MES-NaOH, pH 6.3, and 0.4 M sucrose with either NaCl or NaF depending on the study using the Beckman Avanti J-25 centrifuge. The concentration of the sample was at least 3 mg Chl/mL to be detectable by the EPR. 2 mM PPBQ was added to each sample and 200 µL (about 3 cm heights) of sample was placed into a 4 mm clear fused quartz EPR tube. The sample was then dark adapted by incubation for 45 minutes on ice and was then cooled in 77 K liquid nitrogen.

EPR Spectroscopy

EPR spectroscopy was carried out using a Bruker Instruments EPR spectrometer. Spectra were collected at 77 K using a liquid nitrogen EPR dewar with the microwave frequency at 9.45 GHz, microwave power at 1.0 mW, modulation frequency at 100 kHz,

and modulation amplitude at 3 G. Each spectrum consisting of 4 scans from 3220 G to 3520 G with each scan lasting about 3 minutes.

Both the Tyr_D radical and the Tyr_Z radical are overlapping detectable signals in the EPR spectrum with very similar appearance. The two Tyr residues are present in equal amounts in PSII. The overall Tyr signal can be measured by taking the difference between the maximum at around 3365 G and the minimum at 3358 G. To detect whether the Tyr_Z radical was present in fluoride treated samples, a method was used in which a PSII sample was illuminated to induce both tyrosine radicals, then the PSII sample was placed in the dark for 25 minutes to allow the Tyr_Z signal to decay. After the dark adaptation, the signal consisted of the Tyr_D radical since it takes much longer to decay. The difference between the two signals before and after the decay period gave the intensity of the Tyr_Z radical signal. The EPR experiments using fluoride treated PSII were built around this concept.

In all of the experiments observing the Tyr_Z signal, a method was used that involved different illumination and dark-adaptation times as shown in Table 3. Run 1 was an initial spectrum taken of the dark adapted sample of PSII. This initial condition was the lowest Tyr signal measured, since some of the Tyr_D and all of the Tyr_Z radical decayed during storage. A thawing of the sample in room temperature water for 30 seconds was done. Then upon a 3 to 10 seconds illumination in a 0°C water bath, both the Tyr_D and possibly the Tyr_Z radicals formed. Immediately after the illumination, the sample was first cool in a dry ice and ethanol bath, followed by cooling to 77 K in liquid nitrogen. The spectrum was taken corresponding to run 2. The Tyr_Z radical was

expected to be observable if the electron transfer from the Mn cluster to Tyr_Z was block due to inhibition. For run 3, the sample was thawed in room temperature water followed by a 25 minutes dark adaptation step on ice to allow the Tyr_Z radical to decay, thus leaving only the full Tyr_D radical signal in the EPR spectrum. For run 4, the sample was thawed in room temperature water and a second illumination of 15 seconds to 3 minutes was performed at 0°C to obtain full Tyr_D and possibly the Tyr_Z signals. The PSII sample was immediately cooled again in a dry ice and ethanol bath followed by cooling to 77 K in liquid nitrogen. For run 5, the sample was thawed as before and dark adapted on ice for 25 minutes. This EPR spectrum checked whether the Tyr_Z signal decayed to a level similar to run 3. Table 3 summarizes the sequence of conditions used.

Table 1. Illumination and Dark Adaptation Conditions for EPR of Tyr Radical

Run	Conditions	Tyr Radical Formation
1	Non-illuminated	Some Tyr_D•
2	Short illumination (3-5 seconds)	Full Tyr_D• Some Tyr_Z•
3	25 minutes dark adapt	Full Tyr_D•
4	Long illumination (15 seconds- 3 minutes)	Full Tyr_D• More Tyr_Z•
5	25 minutes dark adapt	Full Tyr_D•

Note: The table shows the experimental conditions for EPR samples given different illumination and dark adaptation times. Also given is the radical formation expected for those conditions.

The equation below shows how the amount of Tyr_Z radical with respect to Tyr_D radical was calculated from illumination and dark adaptation runs given in Table 3. Run

3 was determined to be the most stable signal for 100% Tyr_D radical formation from a study not shown.

$$Tyr\ Z^{\bullet}\% = \left(\frac{\text{Height Run 4 (short illumination)}}{\text{Height Run 3 (25 minute dark adap.)}} - 1\right) \times\ 100$$

CHAPTER IV

RESULTS AND DISCUSSION: CALCIUM AND CHLORIDE DEPENEDENCE OF OXYGEN EVOLUTION BY PSII

The experiments covered in this chapter were designed to understand the interaction of the activators Ca^{2+} and Cl^- in oxygen evolution activity using enzyme kinetic models. The first experiment makes a comparison of the activities of intact PSII and NaCl-washed PSII. Next, the effect of incubation at pH 5.5 is compared to that at pH 6.3 to test for recoverability of activity in NaCl-washed PSII. Finally using various concentrations of Cl^- and Ca^{2+}, the interdependence of the two ions was observed using enzyme kinetics models.

Chloride Dependence of Intact and NaCl-washed PSII

Oxygen evolution assays were conducted for both the intact PSII and the NaCl-washed PSII to test the Cl^- dependence of each. Two concentrations of NaCl were used, 0 mM and 20 mM, where 20 mM NaCl represents a concentration expected to produce full activity of oxygen evolution. In 0 mM NaCl, no activator is available from the buffer, so activity would be due to Cl^- already bound. Figure 6 below shows the results of the assay. Under optimal conditions at pH 6.3, 5 mM Ca^{2+}, and 20 mM NaCl, intact PSII showed a maximum, 100%, oxygen evolution activity of 812 μmol O_2/mg Chl/hr.

Under the same conditions, NaCl-washed PSII activity dropped to 46.4% activity due the loss of the extrinsic subunits from the PSII and/or to other effects of the high salt treatment. NaCl-washed PSII is more dependent on the cofactors Cl^- and Ca^{2+} than intact PSII because of the loss of the extrinsic subunits. With 0 mM Cl^- in the buffer assay, NaCl-washed PSII activity dropped to 6.8%, while intact PSII activity dropped to 54.4%. The intact PSII remained fairly active because both the extrinsic subunits, PsbP and PsbQ, partially prevent the diffusion of ions out from the Mn cluster. The little activity found in NaCl-washed PSII with no Cl^- present may have been due to the trace amount of chloride in the buffer and/or already bound to PSII. In general, intact PSII showed higher activity than NaCl-washed PSII because the presence of the extrinsic subunits is thought to trap Cl^- within the catalytic site. These results also support the proposal that the extrinsic subunits play a major role in the efficiency of oxygen evolution in the PSII protein complex.

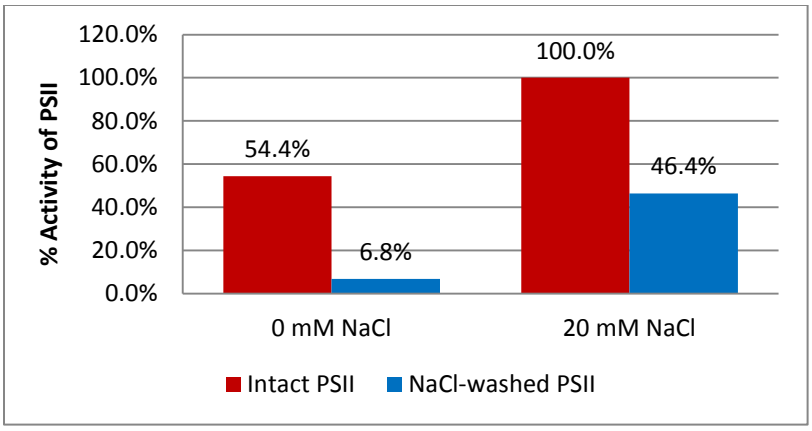

Figure 6. Intact PSII vs NaCl-washed PSII Activity. Comparison of the effect of chloride on O_2 evolution by intact and NaCl-washed PSII in the presence of 5 mM Ca^{2+} at 40 mM MES, pH 6.3, 5 mM Ca^{2+}, and 0.4 M sucrose. The results were graphed as percentage of activity relative to intact PSII with 20 mM NaCl, which showed a rate of 812 O_2/mg Chl/hr.

Recoverability of Activity of NaCl-washed PSII after Treatment at pH 5.5

In anticipation of kinetics experiments to be performed at pH 5.5, treatments of PSII at pH 5.5 were carried out to test for possible damaging effects due to decreasing the pH, as shown in Figure 7. Samples of NaCl-washed PSII were prepared in buffer at one pH, either 6.3 or 5.5, and then assayed at pH 5.5 and 6.3 in buffer containing 0.4 M sucrose, 40 mM MES-NaOH with 20 mM NaCl. The first bar shows the control condition of PSII treated at pH 6.3 and assayed at pH 6.3. This condition resulted in oxygen evolution activity of 390 μmole O_2/mg Chl/hr. The second bar labeled "pH 6.3 to pH 5.5" shows a decrease in oxygen evolution activity to 58% compared to the control sample. The lower activity due to pH 5.5 was too low for optimal activity, but was not due to Cl^- inhibition because the Cl^- concentration was only at 20 mM. The bar labeled "pH 5.5 to pH 6.3" showed a recovered oxygen evolution rate of 98% of the control.

Finally the last bar labeled “pH 5.5 to pH 5.5” showed an oxygen evolution rate that was similar to “pH 6.3 to pH 5.5” conditions. This effect shows that at pH 5.5 the oxygen evolution activity was about half the activity at pH 6.3 whether the sample was incubated at pH 5.5 or not. Upon increasing the pH from 5.5 to 6.3, the oxygen evolution activity did not show damage of PSII due to pH 5.5. Therefore activity in NaCl-washed PSII can recover from treatment at pH 5.5.

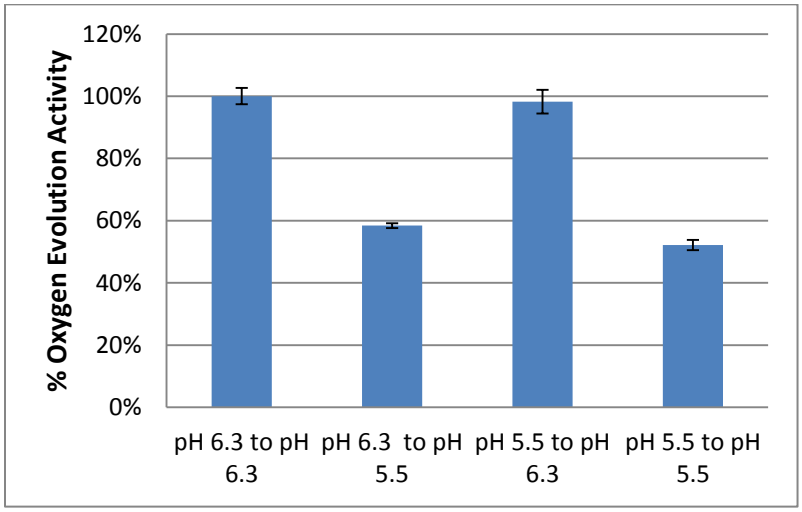

Figure 7. Recoverability of the Activity After Treatment of NaCl-washed PSII at pH 5.5. Oxygen evolution activity in NaCl-washed PSII treated in either pH 6.3 or pH 5.5 buffers, then assayed at pH 6.3 or pH 5.5. 20 mM Cl^- and 5 mM Ca^{2+} was present during treatment and assays.

Chloride Activation of Oxygen Evolution at pH 6.3

In Figure 8, data for chloride activation of NaCl-washed PSII at pH 6.3 and 5 mM Ca^{2+} is shown for increasing chloride concentrations ranging from 0 to 50 mM Cl^-. The effect of chloride may have two possible phases, activation of oxygen evolution and inhibition caused by excessive chloride concentrations. The graph shows an increase in

activity up to a maximum around 20 mM Cl^-. The chloride concentration at half maximum activity was 1.3 mM Cl^-, which corresponds to the Michaelis constant K_m. The data reflect activation by chloride that follows the Michaelis-Menten equation as given in the Background section. There was little or no evidence of inhibition by chloride at high concentrations at this pH.

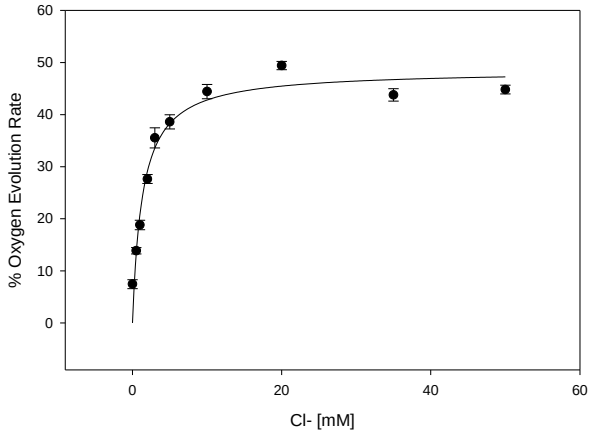

Figure 8. Chloride Activation of Oxygen Evolution at pH 6.3. The graph above shows oxygen evolution activity of NaCl-washed PSII at pH 6.3 with increasing Cl^- concentration in the presence of 5 mM Ca^{2+}. The data were fitted with the Michaelis-Menten equation, giving a K_M of 1.3 mM and V_{Max} of 48%. The 100% activity rate was 408 μmol O_2/mgChl/hr for 20 mM Cl^- and pH 6.3 for intact PSII for this figure.

Chloride Dependence of Activity at pH 5.5 at Various Ca^{2+} Concentrations

A series of oxygen evolution assays was performed at pH 5.5 to examine the effects of both Ca^{2+} and Cl^- simultaneously to determine whether they influence the activation ability of each other. Previous observations in the lab have shown that at pH 5.5 there is an increase in substrate inhibition by chloride, which is inhibition by the substrate or activator from a second binding site. At this pH, the data allowed

examination of the influence of Ca^{2+} on both the site of chloride activation (through K_m) and the site of chloride inhibition (through K_I). In addition, the data set can be used to determine K_m for Ca^{2+} activation as well. The modified enzyme kinetics equation shown below includes a term involving K_I in the denominator to account for the inhibition at higher chloride concentrations (substrate inhibition). An additional constant, V_0, was included to account for activity present at zero chloride, which may be due to trace amounts of chloride in the buffer or bound to PSII.

$$v = \frac{V_{max}\,[Cl^-]}{[Cl^-] + K_m + \frac{[Cl^-]^2}{K_i}} + V_0$$

The data from oxygen evolution assays at pH 5.5 at various chloride and calcium concentrations are showed in Figure 8. Table 2 shows values obtained for individual curves from fits to the substrate inhibition model. The data show that inhibition effects from high concentrations of chloride are present at all concentrations of calcium tested. The fitted values of K_I doubled as the calcium concentration increased, indicating that the inhibition by chloride decreased. At 0.2 mM Ca^{2+} K_I was 31 mM and at 5 mM Ca^{2+} K_I was 68 mM. There was an increase in maximum oxygen evolution activity V_{Max} with increasing Ca^{2+} concentration, as expected for an activator. The Michaelis constant remained constant around 1 mM for all concentration of Ca^{2+} tested.

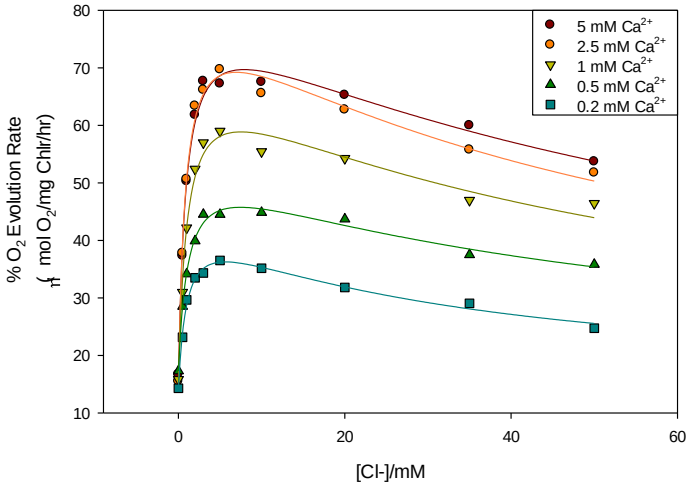

Figure 9. Oxygen Evolution Activity of NaCl-washed PSII in pH 5.5 with Increasing Cl^- Concentrations at Various Concentrations of Ca^{2+}. The data were fitted to the Michealis-Menten equation with substrate inhibition term. All the points were normalized to 100% activity at pH 6.3 with 5 mM Ca^{2+} and 20 mM Cl^-, which showed a rate of 362 µmol O_2/mgChl/hr.

Table 2. Constants from Chloride Dependence of Oxygen Evolution Assays at pH 5.5

Ca^{2+} mM	V_{Max} (% activ.)	K_M (mM)	K_I (mM)	V_o (% activ.)
0.2	30 ± 2	1.0 ± 0.2	31 ± 5	14 ± 1
0.5	37 ± 2	1.2 ± 0.2	48 ± 8	17 ± 1
1	56 ± 3	1.0 ± 0.2	55 ± 14	15 ± 2
2.5	68 ± 3	0.9 ± 0.1	55 ± 9	15 ± 2
5	66 ± 3	0.9 ± 0.1	68 ± 12	16 ± 2

Note: Values of V_{max}, K_M, K_I, V_0, and the standard errors were found from fits to the curves shown in Figure 9.

Bisubstrate Enzyme Kinetics of Chloride and Calcium Activation

To proceed with the bisubstrate kinetics analysis for both Ca^{2+} and Cl^- as substrate, the effect of chloride inhibition was removed from the data. Figure 10 shows the Lineweaver-Burk plots of chloride dependence of oxygen evolution activity, plotted

as 1/v vs 1/[Cl^-]. Also shown superimposed are calculated lines representing the activation portion only, based on the data in Table 2. The experimental values of 1/v decreased with increasing 1/[Cl^-] near the y-axis due to the inhibition effect at high concentrations of chloride. The fitted lines do not show this effect because the inhibition factor, K_I, was omitted in the Lineweaver-Burk fit. The equation for the Linweaver-Burk plot is shown below.

$$\frac{1}{v} = \frac{K_m}{V_{max}[S]} + \frac{1}{V_{max}}$$

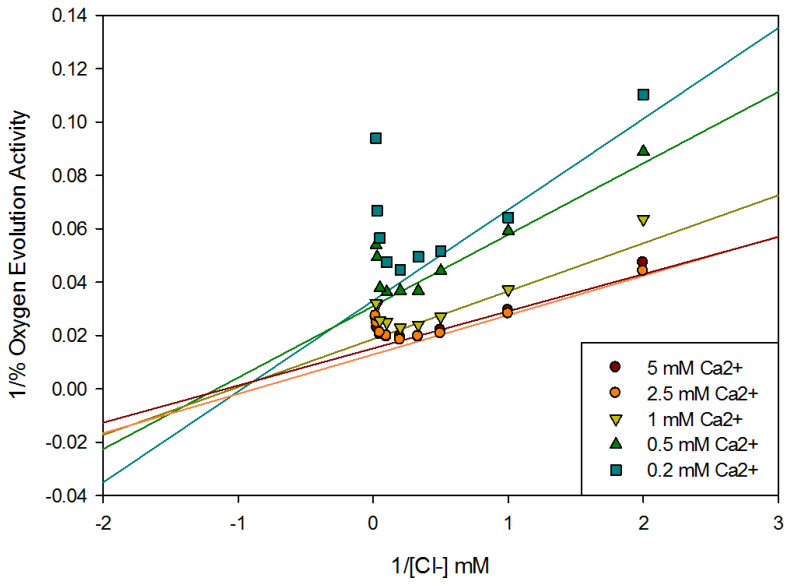

Figure 10. Lineweaver-Burk Plots, 1/v vs 1/[Cl^-]. The experimental points were calculated from the data of Figure 9 superimposed with calculated lines representing the activation portion only (with K_I term omitted).

The next step in the bisubstrate analysis involved the construction of secondary plots obtained from the Lineweaver-Burk plots of Figure 10. Figure 11 shows the y-intercepts of the Lineweaver-Burk plots versus the inverse of the calcium concentration.

Figure 12 shows the slopes of the Lineweaver-Burk plots plotted against the inverse of the calcium concentration. Both of these graphs were fitted to the linear terms that correspond to the appropriate part of the ordered sequential model and the random sequential model as given in the Introduction.

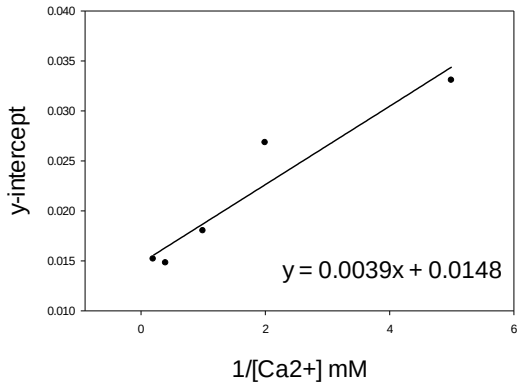

Figure 11. Secondary Plot of y-intercepts of the Lineweaver-Burk Graph. The secondary graph of chloride dependent oxygen evolution assays at pH 5.5, plotting the y-intercepts of the Lineweaver-Burk plots against $1/[Ca^{2+}]$.

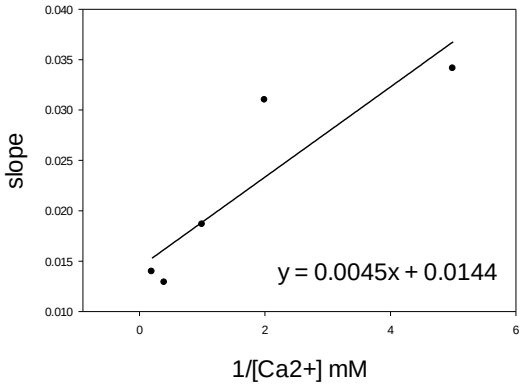

Figure 12. Secondary Plot of the Slopes of the Linewaver-Burk Graph. The secondary graph of chloride dependent oxygen evolution assays at pH 5.5 plotting the slopes of the Lineweaver-Burk plots against $1/[Ca^{2+}]$.

The secondary plots were interpreted in terms of the random sequential binding model and ordered sequential binding model to obtained values of global kinetic

constants as shown in Table 3. The current analysis of the data cannot distinguish between the two models. Both of the models gave the same values since the equation are very similar, although the ordered sequential model can give only one of the two K_S values. The global V_{max} was 68% activity compare to NaCl-washed PSII at pH 6.3, 20 mM Cl^-, and 5 mM Ca^{2+}. The Michaelis constants (K_M) for Ca^{2+} and Cl^- were 0.26 mM and 0.97 mM, respectively, and the dissociation constant for Ca^{2+} was 0.31 mM and for Cl^- was 1.15 mM. Both the Michaelis and the dissociation constants for chloride are higher than those of calcium. Therefore more Cl^- is need for activation of PSII than Ca^{2+}.

Table 3. Global Constants Found from the Random and Ordered Sequential Models

	Random Sequential Model	**Ordered Sequential Model**
V_{Max} (% activ.)	68 ±8	68 ±8
$K_M(Cl^-)$ (mM)	0.97 ±0.32	0.97 ±0.32
$K_S(Cl^-)$ (mM)	1.2 ±0.4	1.2 ±0.4
$K_M(Ca^{2+})$ (mM)	0.26 ±0.06	0.26 ±0.06
$K_S(Ca^{2+})$ (mM)	0.31 ±0.16	--

Note: The table shows the global constants and the standard errors for Ca^{2+} and Cl^- activation were obtained from the fits to the random and ordered sequential binding equations, based on secondary plots shown in Figures 11 and 12.

CHAPTER V

RESULTS AND DISCUSSION: EPR OF FLUORIDE INHIBITED PSII

Fluoride has been previously shown to be a competitive inhibitor of chloride activation of oxygen evolution by PSII. The fluoride inhibition of PSII was studied to determine its relationship to the chloride and calcium requirements at the manganese cluster by observing the Tyr_Z radical formation using EPR spectroscopy. This was accomplished by inducing the tyrosine radical signals under various illumination and dark adaptation conditions. The purpose of the illuminations of PSII was to induce both Tyr_D and Tyr_Z radicals and the dark adaptations were performed to allow the Tyr_Z radical to decay. The first experiment in the study tested the effect of an artificial electron acceptor phenyl-*p*-benzoquinone (PPBQ) by observing Tyr radical intensity using a control sample. Following this preliminary experiment, the effects of multiple illumination and dark adaptation cycles were observed in F^- treated samples to establish the protocol for Tyr_Z measurement. Finally, the main experiment of the study compared treatment with different F^- concentrations in intact PSII and NaCl-washed PSII.

Detecting Tyr Radical Signal

An EPR spectrum of the Tyr radical from a PSII sample is shown in Figure 13. PSII samples were placed into a dewar filled with liquid nitrogen at 77 K, at which the Tyr radical signal was detectable. The Tyr radical signal intensity was calculated from

the difference between the trough at around 3378 G and the maximum at the first peak around 3358 G. The second peak was not used to calculate the Tyr radical because it may include contributions from other radicals such as carotenoids. The errors obtain from the EPR spectrums were calculated using an average of 4 measurements of the height of the noise at the baseline of the EPR signal.

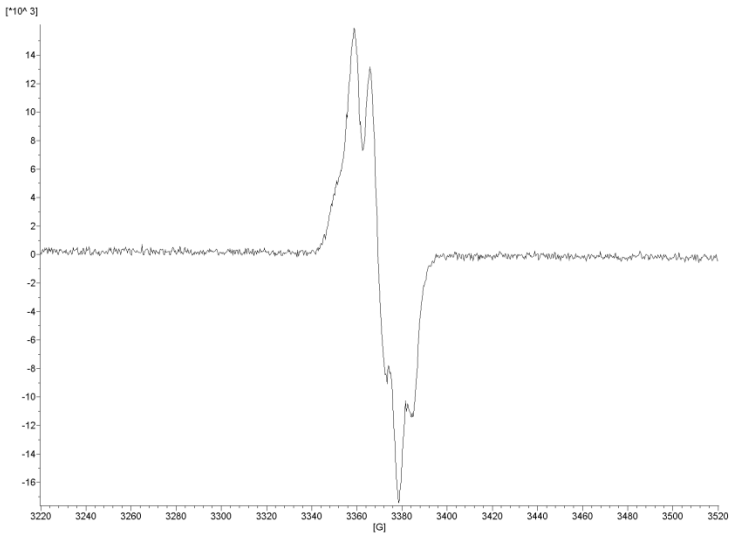

Figure 13. EPR Signal of Tyrosine Radicals. The spectrum was from intact PSII treated with 20 mM NaCl after illumination for 10 seconds at 0°C.

Effect of Electron Acceptor on the Formation of the Tyr Radicals

This following experiment examined whether an artificial electron acceptor helped in observing the Tyr radical formation. Typically electrons entering the electron transfer chain from oxygen evolution in PSII transfer to plastoquinones, Q_A and Q_B. Due to the purification of the PSII sample, Q_B was mostly removed. Phenyl-*p*-benzoquinone (PPBQ) was used as an electron acceptor to allow PSII to go through multiple catalytic turnovers. Figure 14 shows the results of an EPR experiment using intact PSII with and

without the addition of PPBQ. The sequence of runs can be found in Table 1 from the Materials and Methods section. The graph suggests that the addition of PPBQ promotes greater formation of tyrosine radical compared to samples without PPBQ. The intensity of the Tyr_Z radical signal in run 4 with the addition of PPBQ was about twice as high as that with no PPBQ. All other PSII samples for EPR were prepared using 2 mM PPBQ.

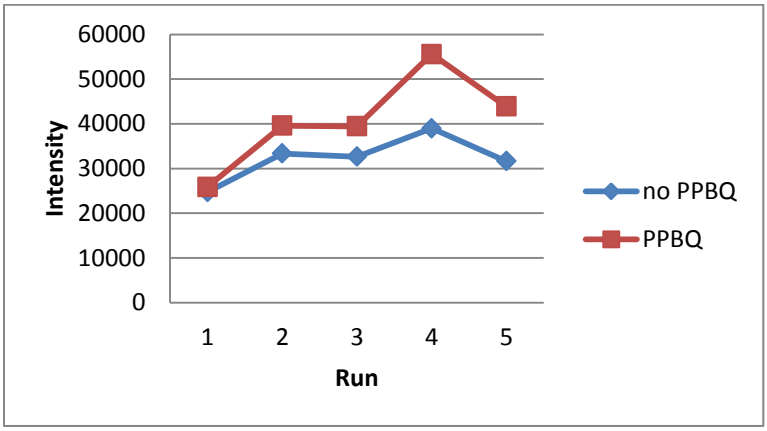

Figure 14. Tyr Radical from Intact PSII with and without PPBQ. The intensity of the Tyr EPR signal at 77 K from control PSII with 2 mM PPBQ and without PPBQ after the sequence of illumination/dark-adaptation conditions described in the text.

Tyr Radical Formation in Intact PSII Treated with High and Low Fluoride Concentrations

Fluoride inhibition in PSII was initially observed for treatment of intact PSII with a low and a high concentration of fluoride. These samples were prepared as described in the Materials and Methods section. The PSII concentrations were between 2.1 and 2.2 mg Chl/mL. Figure 15 shows the effect of fluoride treatment on PSII given similar illumination and dark adaptation conditions to those of Figure 14. This experiment examines the intensity of the Tyr radical signal from PSII samples at concentrations of 20

mM F^- and 150 mM F^-. In general the results for both concentrations of fluoride were similar throughout the illumination and dark adaptation runs with the 150 mM F^- sample showing 53% Tyr_Z radical with respect to Tyr_D radical formation compared to the 45% Tyr_Z radical in the 20 mM NaF treated PSII sample. The increase in F^- concentration appeared to increase the formation of Tyr radical. The dark adaptation from runs 3 and 5 were expected to show the same signal intensity arising from full Tyr_D radical formation, but run 5 showed significantly lower signal than run 3. The 3-minute illumination from run 4 may have caused light-induced damage that led to loss of signal that was seen as a lower intensity in run 5.

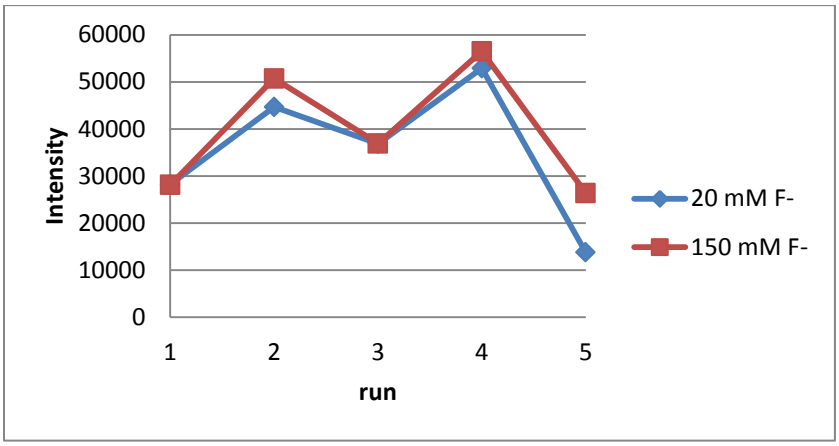

Figure 15. Tyr Radical from Intact PSII Treated with 20 mM NaF and 150 mM NaF. The intensity of the Tyr EPR signal at 77 K was measured after the sequence of conditions described in the text.

Effect of Multiple Illumination and Dark Adaptation Cycles on the Tyr Signal in Intact PSII

The possible light induced damage shown in run 5 of Figure 15 led to an experiment in which the time dependence of illumination was examined to observe any

significant loss of signal that may be due to damage. A control PSII sample (2.6 mg Chl/mL) treated with 20 mM Cl^- and an inhibited PSII sample (2.2 mg Chl/mL) treated with 100 mM F^- were prepared. Tyr radical formation was observed using EPR spectroscopy after various illumination times starting with 5 second with the addition ("+") of 10, 20, and 30 seconds illumination. A dark adaptation of 25 minutes on ice was done between each illumination. Figure 16 shows a graph of the Tyr radical signal measured after the various illumination and dark adaptation conditions. Table 4 shows the intensity values and the corresponding errors from Figure 16.

After multiple illumination and dark adaptation cycles the F^- treated sample showed more Tyr_Z radical compared to the Cl^- treated PSII sample. Both samples showed similar Tyr radical signal intensities after dark adaptation except for the dark adaptation of the F^- treated sample between +20 seconds and +30 seconds illumination. This was probably due to loss of sample while transferring to another EPR tube after the original EPR tube was broken. In general, the two treatments showed similar intensities of stable Tyr_D signal after the dark adaptations. There seemed to be slight light-induced damage after +20 seconds of illumination of the sample as seen as a decrease in Tyr_D radical signal, dark adaptation value, in the 20 mM Cl^- and possibly in the 100 mM F^-. Overall the dark adaptation condition resulted in similar signal intensities in both the 20 mM Cl^- and 100 mM F^- treated PSII samples and the illuminated condition for the 100 mM NaF treated PSII sample resulted in signal intensities that were noticeably higher than in the 20 mM NaCl treated sample.

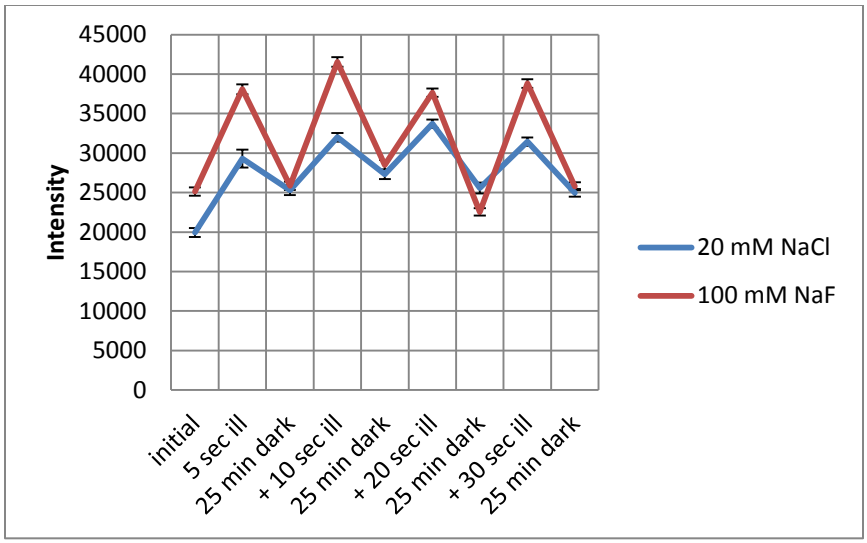

Figure 16. Tyr Radical from Illumination and Dark Adaptation of Intact PSII Treated with 20 mM NaCl and 100 mM NaF. Intensities of EPR signals from Tyr radicals resulting from a time dependent illumination and dark adaptation experiment are shown. Data points from after +20 seconds illumination for the 100 mM NaF PSII sample shows lower intensity due to loss of sample while transferring into a new EPR tube.

Table 4. Tyr_Z Radical from Illumination and Dark Adaptation of Intact PSII Treated with 20 mM NaCl and 100 mM NaF

	20 mM NaCl		100 mM NaF	
Condition	**% Tyr_Z/Ty_D**	**error**	**% Tyr_Z/Ty_D**	**error**
initial	-21.1	± 2.99	-2.8	± 2.84
5 sec ill	15.8	± 5.30	47.3	± 3.82
25 min dark	0.0	± 3.54	0.0	± 2.85
+ 10 sec ill	26.5	± 3.84	60.7	± 4.04
25 min dark	8.0	± 3.60	10.3	± 3.33
+ 20 sec ill	33.3	± 3.94	45.7	± 3.57
25 min dark	1.1	± 3.71	-12.8	± 2.49
+ 30 sec ill	24.2	± 3.74	50.1	± 3.69
25 min dark	-1.3	± 3.15	-0.3	± 2.79

Note: The table shows the intensity of the Tyr_Z radical with respect to the Tyr_D radical based on the first 25 minute dark adaptation as 100% Tyr_D radical. Data correspond to that shown in Figure 16.

Comparison of Tyr Radical in Control and Fluoride Inhibited Intact PSII

To test for reliable tyrosine radical intensity, samples with the same concentrations of NaF or NaCl were tested after illumination and dark adaptation cycles. A control intact PSII sample with 20 mM Cl^- and an inhibited intact PSII with 20 mM F^-, both with PSII concentration of 2.4 mg Chl/mL, were prepared for this experiment. Figure 17 and Table 5 show the Tyr_Z % formation and the error values associated. The short illumination of 5 seconds was used to induce all the Tyr_D radical and Tyr_Z radical. This was followed by a 25 minute dark adaptation to obtain the full Tyr_D radical signal. The second illumination was used to obtain a maximum tyrosine radical signal of both Tyr_D and Tyr_Z which was then followed by a 25 minute dark adaptation, when all Tyr_Z radical was expected to decay leaving the Tyr_D radical. The result expected was that the Tyr radical formation would be higher for the F^- treated sample, however this was not observed in this case. During the "25 min dark 2" condition, the 20 mM NaCl did not show a decrease in Tyr radical intensity compared to the "25 min dark 1." The trend expected was that all the Tyr_Z radical would decay, similar to condition "25 min dark 1." An additional 15 second illumination and dark adaptation was done after storing the sample overnight in liquid nitrogen to confirm the irregular dark adaptation result for the 20 mM NaCl sample. The additional illumination and dark adaptation confirmed the high intensity of Tyr radical formation in the 20 mM NaCl sample, but the cause of the higher intensity is unknown.

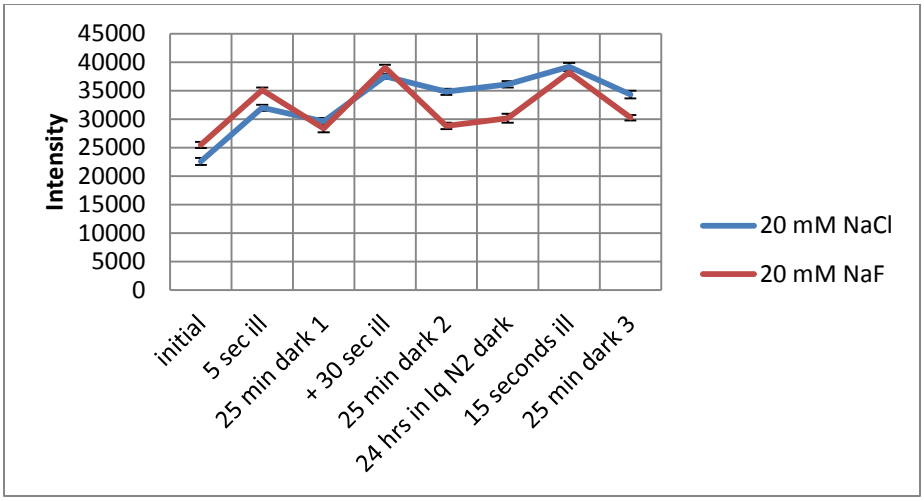

Figure 17. Tyr Radical from Illumination and Dark Adaptation of Intact PSII Treated with 20 mM NaCl and 20 mM NaF. The intensity of the Tyr EPR signal at 77 K is shown after the sequence of conditions described in the text.

Table 5. Tyr_Z Radical from Illumination and Dark Adaptation of Intact PSII Treated with 20 mM NaCl and 20 mM NaF

Condition	20 mM NaCl		20 mM NaF	
	% TyrZ/TyD	error	% TyrZ/TyD	error
initial	-23.7	± 2.57	-10.0	± 2.78
5 sec ill	8.0	± 2.73	23.8	± 3.31
25 min dark 2	0.0	± 2.73	0.0	± 3.24
+ 10 sec ill	26.6	± 2.92	37.6	± 3.60
25 min dark 3	17.5	± 2.88	1.6	± 3.05
24 hrs lq N_2 Dark	21.9	± 3.05	6.5	± 3.72
25 min dark 4	32.3	± 3.45	34.7	± 3.62
+ 30 sec ill	15.8	± 3.18	6.7	± 2.95

Note: The table shows the intensity of the Tyr_Z radical with respect to the Tyr_D radical based on the first 25 minute dark adaptation as 100% Tyr_D radical. Data correspond to that shown in Figure 17.

Tyr EPR Signal in Intact PSII Samples Treated with Increasing Fluoride Concentrations

In the following experiment, the formation of the Tyr_Z radical was observed in samples of intact PSII with increasing concentrations of NaF at 0 mM, 10 mM, 20 mM, 50 mM and 100 mM. These samples, as well as a control sample containing 20 mM NaCl, were prepared as described in the Material and Methods section with concentrations of intact PSII between 2.8 and 3.1 mg Chl/mL. Figure 18 and Table 6 shows the signal intensities of Tyr radicals observed by EPR spectroscopy for the illumination and dark adaptation cycles. This experiment was carried out over 3 days starting on the first day with the 20 mM NaCl and 100 mM NaF samples. On the second day, the 0 mM NaF and 20 mM NaF samples were completed. Finally on the third day, the 10 mM NaF and 50 mM NaF samples were completed.

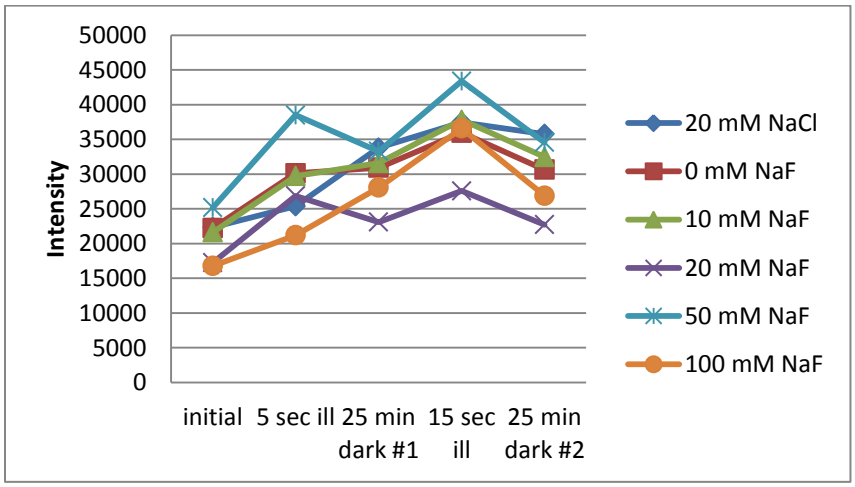

Figure 18. Tyr Radical from Intact PSII with Increasing Fluoride Concentrations. The Tyr_Z radical intensity is shown after the various steps in the illumination and dark adaptation sequence for samples with 0 mM to 100 mM NaF and a control at 20 mM NaCl. PSII concentration was 3 mg Chl/mL for each sample.

Table 6. Tyr_Z Radical from Fluoride Treated Intact PSII

	% Tyr_Z/Tyr_D					
	20 mM NaCl	0 mM NaF	10 mM NaF	20 mM NaF	50 mM NaF	100 mM NaF
Initial	-33.9	-28.1	-31.6	-25.3	-24.4	-40.2
error	3.2	3.7	3.5	5.0	3.5	4.0
5 sec. illum.	-24.9	-2.6	-5.9	16.5	15.8	-24.4
error	3.2	3.9	3.9	6.0	4.5	4.2
25 min. Dark 1	0.0	0.0	0.0	0.0	0.0	0.0
error	3.7	3.8	3.9	5.5	3.9	5.3
15 sec. Illum.	10.8	16.3	19.7	19.5	30.4	30.4
error	4.1	4.7	4.5	6.1	4.6	6.0
25 min. Dark 2	5.8	-0.9	2.8	-1.5	3.9	-4.2
error	3.8	4.1	4.0	5.7	3.8	4.5

Note: The table shows the % Tyr_Z radical with respect to the Tyr_D radical and the corresponding errors were obtained from the data shown in Figure 18.

Tyr_Z Radical from NaCl-washed PSII Treated with Increasing Fluoride Concentrations

The previous experiment showed that intact PSII treated with increasing concentrations of fluoride led to an increase in Tyr Z signal. The extrinsic subunits, PsbP and PsbQ, are present in intact PSII, but are not present in NaCl-washed PSII, where their absence allows easier access of ions such as Ca^{2+} and Cl^-. NaCl-washed PSII samples were prepared with a control at 20 mM Cl^- and various F^- concentrations at 0 mM, 10 mM, 20 mM, 50 mM and 100 mM F^-, with PSII concentration between 2.9 and 3.3 mg Chl/mL. Figure 19 shows a graph of the EPR signal intensity of the tyrosine radical after the illumination and dark adaptation cycles, as for the experiment with intact PSII in Figure 18. Table 7 shows the values obtained from the experiment with the respective

errors obtained from the EPR spectroscopy noise. The experiment was conducted over two days with experiments for samples treated with 20 mM NaCl and 20 mM NaF conducted on one day and experiments for samples treated with 0 mM NaF, 10 mM NaF, 50 mM NaF, and 100 mM NaF conducted on another day.

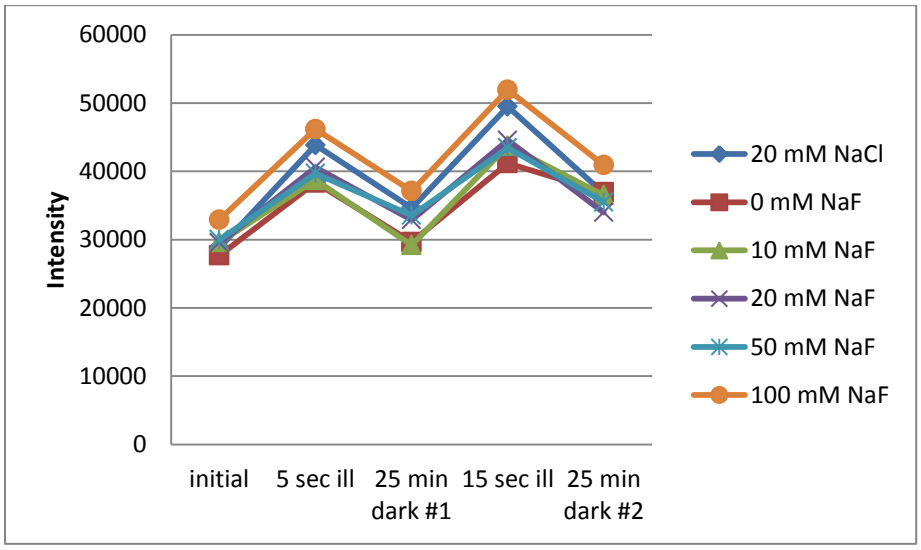

Figure 19. Tyr Radical from NaCl-washed PSII with Increasing Fluoride Concentrations. The Tyr_Z radical intensity is shown after the various steps in the illumination and dark adaptation sequence for samples with 0 mM to 100 mM NaF and a control at 20 mM NaCl. PSII concentration was 3 mg Chl/mL for each sample.

Table 7. Tyr_Z Radical from Fluoride Treated NaCl-washed PSII

	% Tyr_Z/Tyr_D					
	20 mM NaCl	0 mM NaF	10 mM NaF	20 mM NaF	50 mM NaF	100 mM NaF
Initial	-16.7	-6.5	1.4	-10.2	-10.6	-11.3
error	3.0	3.7	4.3	3.0	6.0	3.2
5 sec. illum.	26.7	29.5	32.7	23.4	18.3	24.4
error	4.0	4.4	5.5	3.5	7.4	5.0
25 min. Dark 1	0.0	0.0	0.0	0.0	0.0	0.0
error	3.5	3.8	4.2	3.3	6.4	3.4
15 sec. Illum.	43.0	39.0	49.8	35.4	29.5	39.9
error	4.6	4.8	7.0	4.0	7.3	4.0
25 min. Dark 2	6.2	24.6	25.1	3.3	5.8	10.2
error	3.6	4.3	11.0	3.4	5.9	3.5

Note: The table shows the % Tyr_Z radical with respect to the Tyr_D radical and the corresponding errors were obtained from the data shown in Figure 19.

Comparing Intact PSII and NaCl-washed PSII Treated with Increasing Fluoride Concentrations

The results of Tyr_Z radical signal measurements from intact and NaCl-washed PSII with increasing F^- concentration are shown in Figure 20. The data for intact PSII shown in blue appears to have a positive correlation of Tyr_Z radical formation with increasing F^- concentration, as noted above. The Tyr_Z radical formation appears to reach saturation of about 36% Tyr_Z with respect to the Tyr_D radical starting around 50 mM F^-. The data for the NaCl-washed PSII does not appear to be correlated with increasing F^- concentration as in intact PSII. This effect may be caused by the lack of calcium in the NaCl-washed PSII samples. NaCl-washed PSII is more sensitive to ions from the buffer since the extrinsic subunits, PsbP and PsbQ, are absent. These extrinsic subunits are

known to provide an ion diffusion barrier to the manganese cluster. When the subunits are absent, the addition of Ca^{2+} to the buffer is required for full activity. However the addition of Ca^{2+} to the buffer along with F^- is complicated because of the likely formation of insoluble CaF_2. In addition the lack of calcium in the NaCl-washed PSII used here may have resulted in additional inhibition of oxygen evolution due to a blockage of electron transfer from the Mn cluster, similar to F^- treated PSII. The lack of calcium and the presence of fluoride may both be factors that increased formation of the Tyr_Z radical.

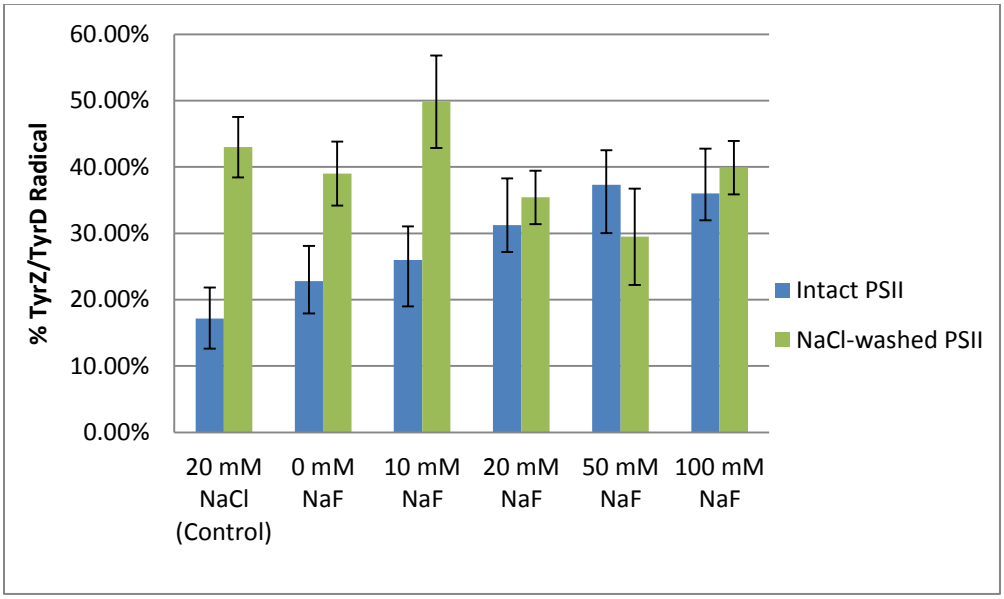

Figure 20. Comparison of Tyr_Z Radical in Intact PSII and NaCl-washed PSII with Increasing Amounts of Fluoride. The Tyr_Z radical intensities are shown in blue for intact PSII and in green for NaCl-washed PSII, alongside a control with 20 mM NaCl for each.

CHAPTER VI

CONCLUSION

Oxygen evolution by PSII in higher plants requires activation by both calcium and chloride. Through an enzyme kinetics study at pH 5.5, chloride was found to cause inhibition of oxygen evolution at high concentrations. The inhibition due to high chloride was also effected by the concentration of calcium. Increasing the calcium concentration at pH 5.5 lowered the inhibition effect cause by high concentrations of chloride. Through bisubstrate analysis of Ca^{2+} and Cl^- activation, chloride was found to show higher Michaelis and dissociation constants for oxygen evolution compared to calcium. The enzyme kinetics study overall determines the details of the relationship between the cofactors, Ca^{2+} and Cl^-, during catalytic formation of molecular oxygen.

Fluoride, a competitive inhibitor of chloride activation, showed inhibition of oxygen evolution resulting in formation of the Tyr_Z radical, as observed through EPR spectroscopy. The results of the EPR experiment showed that increasing concentrations of fluoride had a positive correlation with the formation of the Tyr_Z radical in intact PSII. The study also suggested that PSII preparations lacking in sufficient calcium may show effects on the formation of Tyr_Z radical. The fluoride inhibited study validates the use of the Tyr_Z signal at 77 K for studies in the future without the need to depend on liquid helium to observe the $S_2Y_Z^{\bullet}$ signal.

Further possible investigation of the interaction of calcium and chloride during oxygen evolution in PSII includes observation of the Tyr_Z radical using NaCl-washed PSII samples prepared with an adequate amount of calcium in the buffer. This may reduce the increase of Tyr_Z radical formation caused by depletion of calcium in the manganese cluster. In contrast to avoiding Tyr_Z radical formation due to calcium depletion, another possible experiment for further investigation would be to induce the Tyr_Z radical formation by depleting the sample of calcium. The two results could be compared with those of fluoride inhibited NaCl-washed PSII samples to reveal factors that influence the formation of the Tyr_Z radical.

REFERENCES

Ayala, I., Kim, S., and Barry B. (1999) A difference fourier transform infrared study of tyrosyl radical z decay in photosystem II. Biophysical Journal 77: 2137-2144.

Arnon, D. (1949) Copper enzymes in isolated chloroplasts. Polyphenol oxidase in *Beta vulgaris*. Plant Physiology 24: 1-15.

Barry, B. (1995) Tyrosine radicals in photosystem II. Method Enzymol. 258: 303-319.

Barry, B. and Babcok G. (1984) Tyrosine radical are involved in the photosynthetic oxygen-evolving system. Proc. Natl. Acad. Sci. USA. 84:7099-7103.

Barry, B. and Babcock G. (1987) Tyrosine radicals are involved in the photosysnthetic oxygen-evolving system. Proc. Natl. Acad. Sci. USA 84: 7099-7103.

Baumgarten, M., Philo, J., and Dismukes, G. (1990) Mechanism of Photoinhibition of Photosynthetic water oxidation by Cl- depletion and F- substitution: oxidation of a protein residue. Biochemistry 29:10814-10822.

Berthold, D. A., Babcock, G. T., and Yocum, C. F. (1981) A highly resolved, oxygen-evolving photsystem II preparation from spinach thylakoid membranes. FEBS Lett. 134: 231-234.

Boussac, A., Ishida, N., Sugiura, M., and Rappaport, F. (2012) Probing the role of chloride in Photosystem II from *Thermosynechococcus elongates* by exchanging chloride for iodide. Biochemica et Biophysica Acta 1817: 802-810.

Bryson, D., Doctor, N., Johnson, R., Baranov, S., and Haddy, A. (2005) Characteristics of Iodide Activition and Inhibition of Oxygen Evolution by Photosystem II. Biochemistry 44:7354-7360.

Cammarata, K. and Cheniae, G. (1987) Studies on 17, 24 kD depleted photosystem II membranes. Plant Physiol. 84: 587-595.

Dau, H. and Haumann, M. (2007) The manganese complex of photosystem II in its reaction cycle-Basic framework and possible realization at the atomic level. Coordination Chemistry Review 252: 273-295.

DeRose, V., Latimer, M., Zimmermann, J., Mukerji, I., Yachandra, V., Sauer, K., and Klein, M. (1995) Fluoride substitution in the Mn cluster from photosystem II: EPR and X-ray absorption spectroscopy studies. Chemical Physic 194: 443-459.

Haumann, M., Mulkidjanian, A., and Junge, W. (1999) Tyrosine-Z Oxygen-Evolving Photosystem II: A Hydrogen-bonded Tyrosinate. Biochemistry 38: 1258-1267.

Hillier, W. and Babcock, G. (2001) Photosynthetic reaction Centers. Plant Physiol. 125:33-37.

Ifuku, K., Ido, K., and Sato, F. (2011) Molecular function of PsbP and PsbQ proteins in the photosystem II supercomplex. Journal of Photochemistry and Photobiology B: Biology. 104:158-164.

Kakiuchi, S., Uno, C., Ido, K., Nishimura, T., Noguichi, T., Ifuku, K., and Sato, F. (2012) The PsbQ protein stabilizes the functional binding of the PsbP protein to photosystem II in higher plants. Biochim Biophys Acta. 1817:1346-1351.

Kawakami K, Umena Y, Kamiya N, and Shen J. (2009) Location of Chloride and its Possible Functions in Oxygen-Evolving Photosystem II Revealed by X-ray Crystallography. PNAS 106 (21):8567-8572.

Kawakami K, Umena Y, Kamiya N, and Shen J. (2011) Structure of the catalytic, inorganic core of oxygen-evolving photosystem II at 1.9 Å resolution. Journal of Photochemistry and Photobiology B: Biology 104: 9-18.

Kern, J., and Renger, G. (2007) Photosystem II: Structure and mechanism of the water: plastoquinone oxidoreductase. Photosynth Res. 94:183-202.

Kok B, Forbush B, and McGloin M. (1970) Cooperation of charges in photosynthetic O_2 evolution-I. Photochem Photobiol 11(6):457-75.

Kuntzleman, T. and Haddy, *A.* (2009) Fluoride Inhibition of Photosystem II and the Effect of Removal of the PsbQ Subunit. Photosynthesis Research**.** 102: 7-19.

Marangoni, A. Enzyme Kinetics: A Modern Approach. John Wiley & Sons. Inc, Hoboken, 2003.

Miyao, M. and Murata, N. (1985) The Cl^- effect on photosynthetic oxygen evolution: interaction of Cl- with 18-kDa, 24-kDa and 33-kDa proteins. FEBS Lett. 180:303-308.

Saito, K., Shen, J., Ishida, T., and Ishikita, H. (2011) Short Hydrogen Bond between Redox-Activie Tyrosine Yz and D1-His190 in the Photosystem II Crystal Structure. Biochemistry 50(45): 9836-9844.

Saito, K., Rutherford. A, and Ishikita, Hiroshi. (2013) Mechanism of tyrosine D oxidation in Photosystem II. Proc. Natl. Acad. Sci. USA. 110(19): 7690-7695.

Schönknecht, G., Neimanis, S., Katona, E., Gerst, U., and Heber, U. (1995) Relationship between photosynthetic electron transport and pH gradient across the thylakoid membrane in intact leaves. Proc. Natl. Acad. Sci. USA. 96: 12185-12189.

Seidler, A. (1996) The extrinsic polypeptides of photosystem II. Biochim Biophys Acta 1277:35-60.

Smith, B., Morrissey, P., Guenther, J., Nemson, J., Harrison, M., Allen, J., and Melis, A. (1990) Response of the photosynthetic apparatus in dunaliella salina (green algae) to irradiance stress. Plant Physiol. 93:1433-1440.

Umena, Y., Kawakami, K., Shen, J., and Kamiya, N. (2011) Crystal structure of oxygen-evolving photosystem II at a resolution of 1.9 A. Nature 473:55-60.

Vinyard, D., Ananyev, G., and Dismukes, G. (2013) Photosytem II: The Reaction Center of Oxygenic Photosynthesis. Annu. Rev. Biochem. 82: 577-606.

Yocum, C. F. (2007) The calcium and chloride requirement of the O_2 evolving complex. Coordination Chemistry Reviews 252: 296-305.